Energy for Sustainable Development 31 (2016) 185–193

Contents lists available at ScienceDirect

Energy for Sustainable Development

Tests on two small variable pitch cross flow hydrokinetic turbines

Brian Kirke *

Barbara Hardy Institute, University of South Australia, GPO Box 2471, Adelaide 5001, South Australia

ARTICLE INFO

Article history:
Received 20 September 2014
Accepted 1 February 2016
Available online xxxx

Keywords:
Hydrokinetic turbine
Cross flow
Variable pitch
Reynolds number

ABSTRACT

Cross flow hydrokinetic turbines (HKTs) have some advantages and some disadvantages compared to axial flow HKTs. Fixed pitch cross flow HKTs suffer from lack of starting torque, torque ripple and shaking. It has been shown theoretically that these problems can be greatly reduced by means of variable pitch, but there is very little experimental data available on the actual performance of variable pitch HKTs. Two small cross flow hydrokinetic turbines with sinusoidally pitching straight blades were tested by driving them through still water to simulate a stationary deployment in a tidal flow. A 1 m diameter turbine with a passive eccentric mechanism was tested in open water, and a 0.5 m diameter turbine with cam-driven pitch was tested in a laboratory tow tank. A strong Reynolds number effect was observed, with peak performance coefficients ranging from 0.1 for the 0.5 m diameter turbine at 0.5 m/s in the towing tank, up to about 0.32 for the 1 m diameter turbine in open water at about 1 m/s, suggesting that larger turbines can be expected to perform better. CFD and streamtube predictions are compared with experimental data. Two-dimensional predictions, i.e. those ignoring parasitic drag loss, are shown to over-predict performance, and there is a need for modeling that accounts for these losses.

Introduction

Hydrokinetic turbines (HKTs) are analogous to wind turbines in that they convert kinetic energy in a moving fluid to mechanical shaft energy, but they do so in water rather than in air. Cross flow turbines in which the fluid flow is essentially normal to the axis of rotation are commonly referred to as "vertical axis" turbines because the axis of rotation is usually vertical as shown in Fig. 1, but it may be oriented horizontally—see for example the Ocean Renewable Power Company (ORPC) turbine (http://www.orpc.co).

Although the fluid dynamic principles governing the behavior of HKTs are in most respects the same as for wind turbines, there are some significant differences:

(i) Unlike wind turbines where the only limitations on blade speed are mechanical stress and noise level, HKT blade speed through the water is limited to about 10 m/s due to the danger of cavitation, although this limit depends to some extent on several factors such as blade cross section, lift coefficient and depth of submergence. This places a limit on tipspeed ratio λ, especially at sites with high flow velocities and corresponding high power density which are the most economically attractive. The factors influencing the onset of cavitation are discussed in (Batten et al., 2008). Cavitation problems can be reduced by (i) selecting a suitable blade profile which does not develop a high peak suction pressure, (ii) maintaining a low angle of attack, (iii) reducing the blade speed by reducing the tipspeed ratio, and (iv) increasing the depth of submergence.

(ii) Because the density of water is about 830 times higher than that of air and ambient flow velocities are typically several times lower than the wind velocities necessary for wind turbines to be viable, fluid dynamic forces on hydrokinetic turbine blades typically exceed inertial forces, unlike those on small wind turbines. This has implications for the structural design of blades and for the design of passive pitch control systems, since these systems on vertical axis wind turbines commonly use inertia to stabilize blade pitch (Kirke and Lazauskas, 2011), but this is not practicable for HKTs since inertial forces are very much lower.

Cross flow HKTs

The advantages and disadvantages of cross flow versus axial flow HKTs have been discussed by numerous authors—see for example (Kirke and Lazauskas, 2011), but for convenience are recapped here. Oriented with the shaft vertical, cross flow HKTs have at least four major advantages over axial flow HKTs:

(i) They are insensitive to flow direction unless they have a pitch control system which requires orientation to the flow
(ii) The gearbox (if used) and generator can be located above water level or just below the surface where they are easily accessible for maintenance
(iii) Several mass-produced, manageable sized turbines can be stacked in modular fashion on the same shaft to produce power equivalent to a single large turbine

* Tel.: +618 81651608.
E-mail address: brian.kirke@unisa.edu.au.

http://dx.doi.org/10.1016/j.esd.2016.02.001
0973-0826/

Notation

A	turbine swept area
c	blade chord length
C_p	performance coefficient or power coefficient = fraction of incident kinetic energy flux converted to shaft power $P/(½\ \rho\ A\ V_{inf}^3)$
n	number of blades
P	power
r	turbine radius
Re	blade chord Reynolds number = $V_{rel}\ c/\nu$
T	torque
TSR	tipspeed ratio = λ
V_b	blade speed = Ωr
V_{inf}	towing speed
V_{rel}	blade velocity relative to water
α	angle of attack
γ	pitch amplitude
λ	tipspeed ratio = V_b / V_{inf}
ν	kinematic viscosity
ρ	water density
σ	solidity = nc/r
Ω	angular velocity

(iv) Having a rectangular swept area, cross flow turbines with straight blades can be close-packed more effectively than axial flow turbines, resulting in increased turbine efficiency and tidal farm power (Willden and Nishino, 2014; Cooke et al., 2014).

Although various cross flow HKT designs have been proposed, some based on the Savonius or "S rotor" and some based on other drag type machines, these are inherently material-intensive and inefficient, and the straight blade Darrieus geometry shows the most promise for large scale power generation.

The biggest drawbacks of the fixed pitch Darrieus geometry are

(i) Blade stall, leading to low or negative torque at low λ, necessitating motor start or a hybrid Savonius–Darrieus configuration in tidal streams which stop and reverse four times per day. This arrangement has been used on Darrieus wind turbines like the one as shown in Fig. 2, which was tested at the Weapons Research Establishment (now DRCS), Salisbury, South Australia in the late 1970s (Robinson, 1981). The Savonius rotor provides starting torque and the Darrieus generates power at operating tipspeed ratios. This system has not to the author's knowledge been used on HKTs.

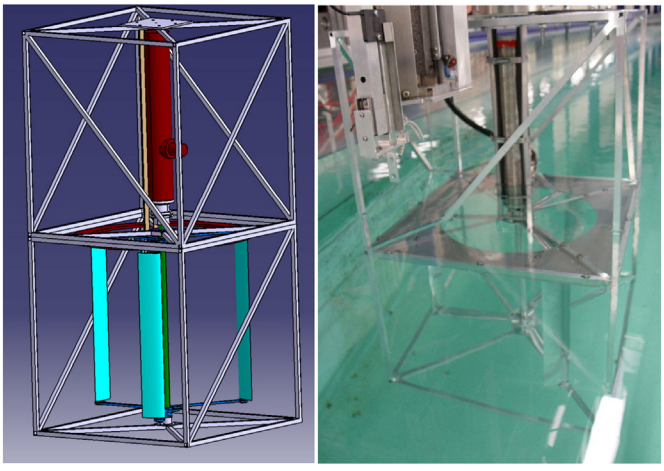

Fig. 1. Vertical axis HKT model test rig: CAD drawing left, and turbine in towing tank at right.

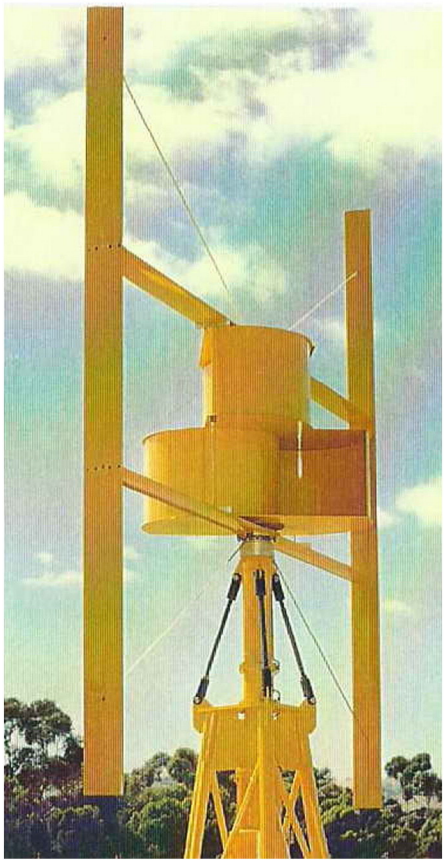

Fig. 2. A hybrid Savonius–Darrieus wind turbine.

(ii) Fluctuating radial and tangential forces on blades, leading to torque ripple and shaking of the turbine, especially at low tipspeed ratios where blades stall twice per revolution. For example the speed of the wind turbine shown in Fig. 2 had to be limited due to severe shaking (Robinson, 1981). By pitching blades so as to reduce or limit stall, variable pitch can ensure adequate starting torque and can substantially reduce radial and tangential force fluctuations (Lazauskas and Kirke, 2012).

Pitching blades to avert or minimize stall

Fig. 3 after Lazauskas (2008) shows how the angle of attack α of a fixed pitch Darrieus turbine varies with azimuth angle θ as tipspeed ratio λ increases, and the pitch amplitude γ necessary to limit α to 10° and hence avoid stall, assuming a stall angle of 10°. While this is only a typical figure for low Re operation and does not take into account Re effects (higher stall angle at higher Re—see Fig. 4) or dynamic stall effects which increase the stall angle when α is increasing and decrease it when α is decreasing, it gives a general indication of the fact that the required pitch amplitude decreases as λ increases.

It follows that it is desirable to vary the pitch amplitude if the turbine is to operate at varying λ, for example for a large wind turbine with a lot of inertia which is unable to vary its speed quickly to track sudden short term gusts and lulls and so maintain constant λ (although modern wind turbines do operate at varying speed to track more long-term changes in wind speed). But the velocity of river and tidal flows in which HKTs operate changes only slowly (unless the flow is highly turbulent, in which case it is probably impossible to track changes in velocity). Thus a maximum power point tracker should be able to vary the

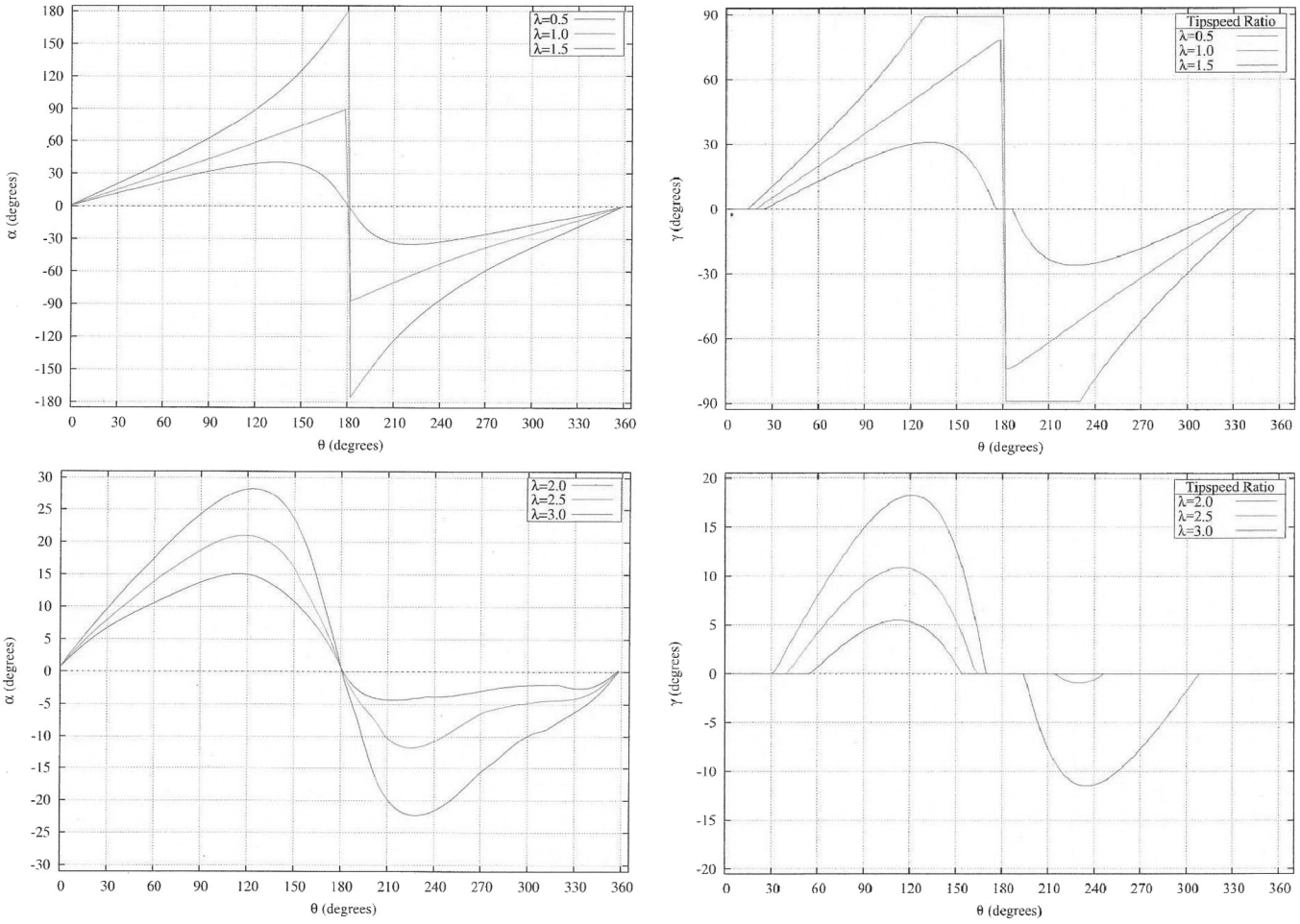

Fig. 3. Variation in α with θ for a fixed pitch turbine at various λ, and the corresponding pitch angles γ required to prevent α exceeding 10°.

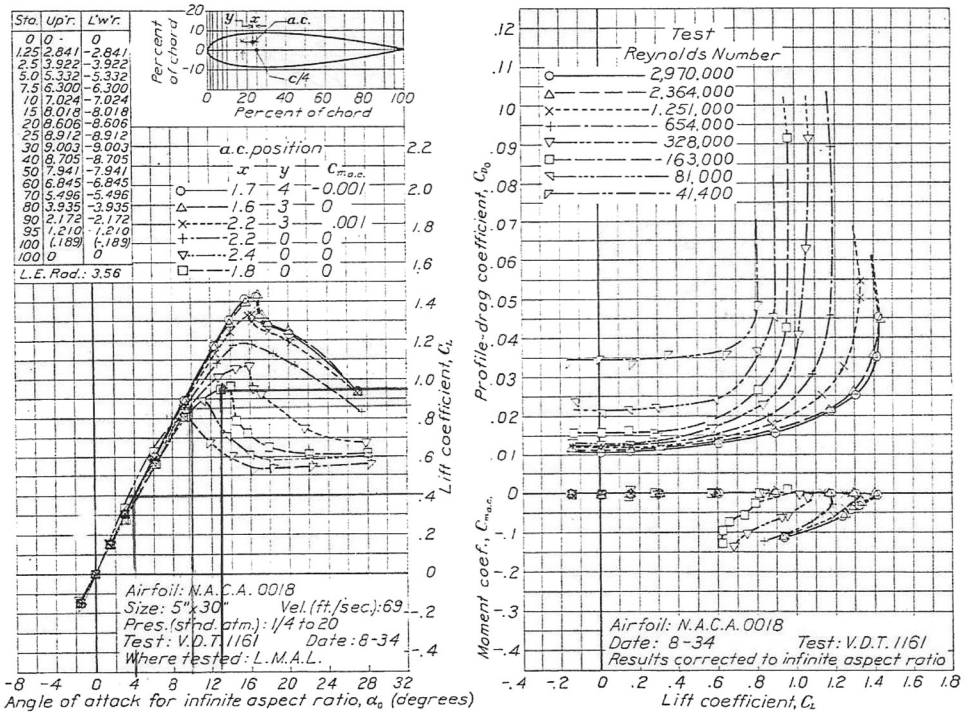

Fig. 4. Stall angle and maximum lift coefficient decrease steeply, and zero incidence drag coefficient increases steeply at low Re (after (Jacobs and Sherman, 1937)).

electrical load so as to vary the HKT speed and maintain constant λ, in which case only one pitch amplitude is required and a simple system will suffice. Two questions then arise:

First, what is the optimum pitch regime? Will a simple sinusoidal pitching action be adequate, or is a more complex regime preferable? Fig. 5 shows a series of possible pitch regimes modeled by Lazauskas (2008), in which the pitch system is defined by

$$\gamma(\theta) = C_1 + \sum_{j=2}^{M} C_j \sin[(j-1)\theta] \quad (1)$$

where the C_i are constants to be found by a Memetic Algorithm optimization process. Predicted C_P–λ curves for values of M from 2 to 6 are shown in Fig. 6. Thus, for M = 2, a simple sinusoidal pitch regime, we have

$$\gamma(\theta) = C_1 + C_2 \sin\theta. \quad (2)$$

Fig. 6 indicates that sinusoidal pitching can produce a big improvement over fixed pitch, but little is gained by the more complex pitching regimes shown in Fig. 5. For j = 2, the optimum values for maximum C_p were found to be $C_1 = 1°$ and $C_2 = 7°$ for this particular turbine geometry. For turbines of higher solidity, which reach maximum C_P at lower λ (Kirke and Lazauskas, 2011), the optimum pitch amplitude will be larger, and conversely for turbines of lower solidity which reach maximum C_P at higher λ, the optimum pitch amplitude will be less.

Pitch control systems

It is one thing to decide on a desirable pitch regime, but quite another to design a robust, economical mechanism that will achieve this desirable pitch regime. Numerous pitch control systems have been proposed, ranging from simply pivoting blades near their leading edge so they are free to pitch within limits (Kentfield, 1985; Coiro et al., 2005) to sophisticated systems with sensors, microprocessors and stepper motors to control blade pitch (Brulle, 1977; Kaare and Evensen, 2003).

Sinusoidal pitch

A simple eccentric will produce a sinusoidal pitch regime, and the patented (Kirke) design shown in Fig. 7 automatically orients itself to the current direction. Each blade is pivoted near its leading edge so it pitches trailing edge downstream on both its upstream and downstream passes due to fluid dynamic forces like the mainsail of a yacht sailing in circles, thus reducing the angle of attack α and reducing or averting stall. Pitch amplitude γ (i.e. C_2 in Eq. (1)) is limited by means of control arms connecting each blade near its trailing edge to a ring which rolls around the central shaft with enough clearance to allow the required pitch amplitude. The offset C_1 is achieved simply by adjusting the length of these control arms.

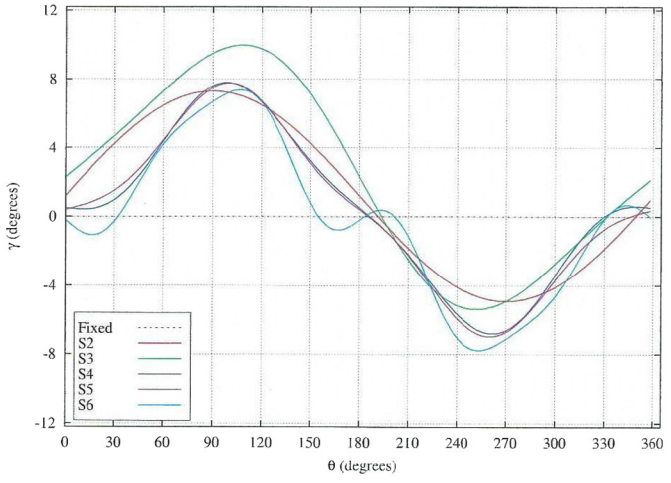

Fig. 5. Optimum pitch amplitudes for a cross flow turbine of solidity nc/r = 0.6 at TSR = 2.5, for various pitching regimes, after (Lazauskas, 2008).

Cam-driven pitch

A cam can achieve any pitch regime (within limits), so could in principle achieve slightly higher peak C_P, as shown in Figs. 5 and 6. However the cam must then be oriented relative to the flow.

Controlled angle of attack

To optimize the pitch regime over a range of λ, it is necessary either to

(i) sense both current speed and angular velocity Ω, hence calculate λ and hence the desired pitch regime for that value of λ, then use stepper motors to drive this pitch regime, or
(ii) sense the instantaneous α on each blade and use stepper motors to drive this pitch regime.

Selection of pitch system

Both sinusoidal and single cam systems can be optimized for one λ only, but as argued above, it should be possible to maintain a constant λ by sensing current speed and angular velocity Ω and controlling Ω by varying the electrical load. Thus this need not be a disadvantage for HKTs where the current speed is changing only slowly.

For the open water tests conducted in South Australia it was decided that an offset sinusoidal pitch regime as shown in Fig. 7 would offer the best combination of simplicity and adequate performance, while a cam was adopted for the towing tank tests conducted by Cranfield University in the UK.

Experimental rigs

South Australian turbine construction and testing

The SA turbine, shown in Fig. 8, was 1 m diameter × 1.2 m high, the largest that could fit between the hulls of the test platform, with 3 straight aluminum blades of 100 mm chord length, CNC milled to NACA 0020 profile, pivoted on radial arms at top and bottom of 60 mm chord, also of NACA 0020 profile, bolted to hubs on a central shaft of 32 mm OD steel tube. Vesconite, an elastomeric low friction plain bearing material used for marine propeller shaft bearings, was used for the lower bearing which was immersed in water, while ordinary deep groove ball bearings were used at the top, above water level. One bearing, hidden by the sprocket in Fig. 8, held the shaft while a geared DC generator was mounted on a frame free to rotate on the pair of bearings visible in Fig. 8 and driven via a chain and sprockets. The reaction torque on the turbine shaft was measured by means of a Coti 1 kN load cell attached to the generator frame, and a reed switch registered a pulse each time a magnet attached to the sprocket on the turbine shaft passed. A Swoffer propeller type flow velocity meter was mounted on a long arm extending out in front of the catamaran to measure turbine speed through the water. The speed, torque and time between pulses were logged on a purpose-built data logger and downloaded in real time to a laptop for processing.

In early tests the catamaran was pushed in front of the power boat and in later tests it was towed, using its rudders to keep it well to one side to minimize turbulence from the wake of the tow boat. The boat was driven at as near as possible steady speed and a variable resistive dummy load on the generator was used to vary the load torque. A

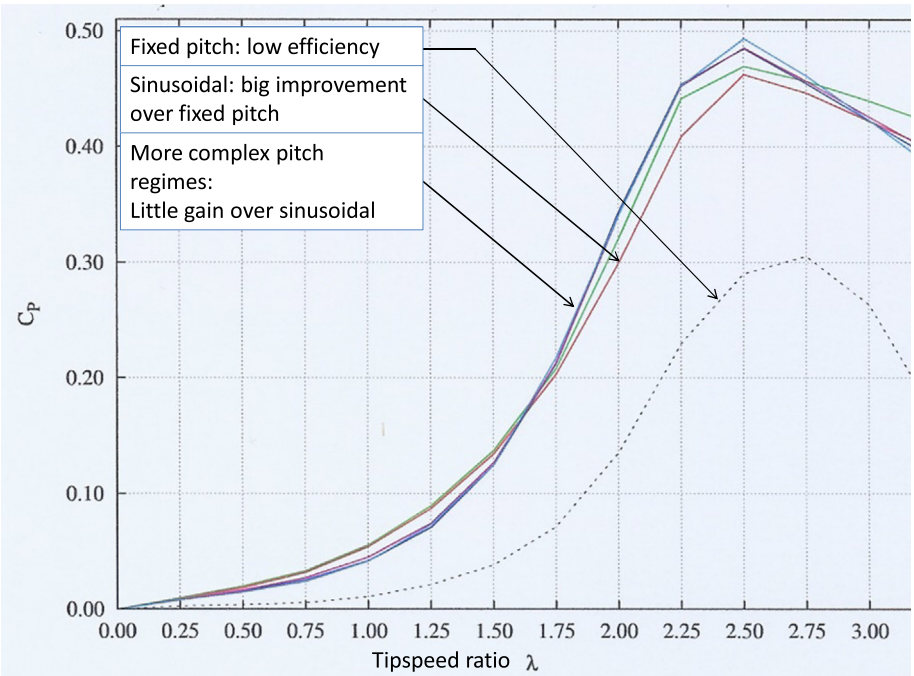

Fig. 6. Sinusoidal pitching is a big improvement over fixed pitch but little is gained by more complex pitching regimes, after (Lazauskas, 2008). Colors correspond to values of M shown in Fig. 5. (For interpretation of the references to color in this figure legend, the reader is referred to the web version of this article.)

gradual slight variation in boat speed did not matter because torque was logged at 10 ms intervals, boat speed at 2 s intervals and turbine speed every revolution. The turbine was tested at speeds ranging from 0.6 to 2 m/s.

UK turbine construction and testing

A 0.5 m diameter turbine, shown in Fig. 1, was designed by the present author and tested in a 1.5 × 1.5 m section laboratory towing tank at Cranfield University, UK. It was of similar construction to the SA turbine, but was 0.5 m diameter × 0.5 m high, with blades of 70 mm chord length, pivoted on radial arms of 30 mm chord. Radial arms were made as thin as practicable to minimize parasitic drag. Since solidity $\sigma = nc/r = 3 \times 0.07/0.25 = 0.84$, slightly higher than that of the SA turbine which was modeled by (Lazauskas, 2008), it was expected to reach peak C_p at a slightly lower λ so a larger sinusoidal pitch amplitude of 2° ± 9.5° was used. The turbine size was limited by the dimensions of the towing tank and the towing velocity was limited to 1.15 m/s by the maximum available towing force of 200 N. Such a small turbine proved to be very fragile.

The turbine was mounted in a braced frame as shown in Fig.1, which was fixed below the motor-generator unit (shown red in Fig. 1, left) under the towing carriage. For each test run the turbine was towed at a steady speed and torque output T was logged for a series of angular velocities Ω. The towing speed V_{inf} was then increased and the process repeated. Speeds ranged from 0.5 to 1.15 m/s. From the angular velocity the blade speed V_b was calculated, and hence λ was calculated.

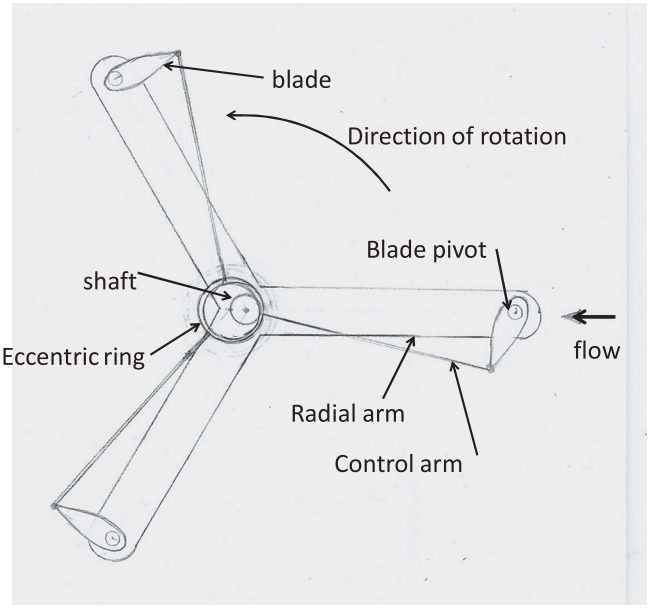

Fig. 7. Eccentric ring pitch control system used on the South Australian turbine.

Results

Power output P and performance coefficient C_p were calculated from the following relations:

$$P = T\omega \tag{3}$$

$$C_p = P/({}^1/_2\rho\ A\ V_{inf}{}^3) \tag{4}$$

where ρ = water density = 1000 kg/m^3 (fresh water in lab) or 1025 kg/m^3 (sea water), and swept area A = 1.2 m^2 for the SA tests and 0.25 m^2 for the UK tests. The resulting C_p–λ curves are shown in Figs. 9 and 10. Shown also in Fig. 10 is the range of blade chord Re encountered at each data point. Blades experience a higher Re when moving upstream than when moving downstream, so Re = 0 when a blade is moving directly downstream at λ = 1. However most of the power is produced when the blade is moving upstream and across the flow upstream, where Re is close to the upper limits shown in Fig. 10. There were no obvious Re effects in the SA tests where Re ranged from about 150,000 to 350,000 at λ = 2.5, with most of the power produced in the upper range.

In the Cranfield tests the peak power coefficients ranged from 0.1 to 0.31, increasing steadily with increasing Reynolds numbers, showing

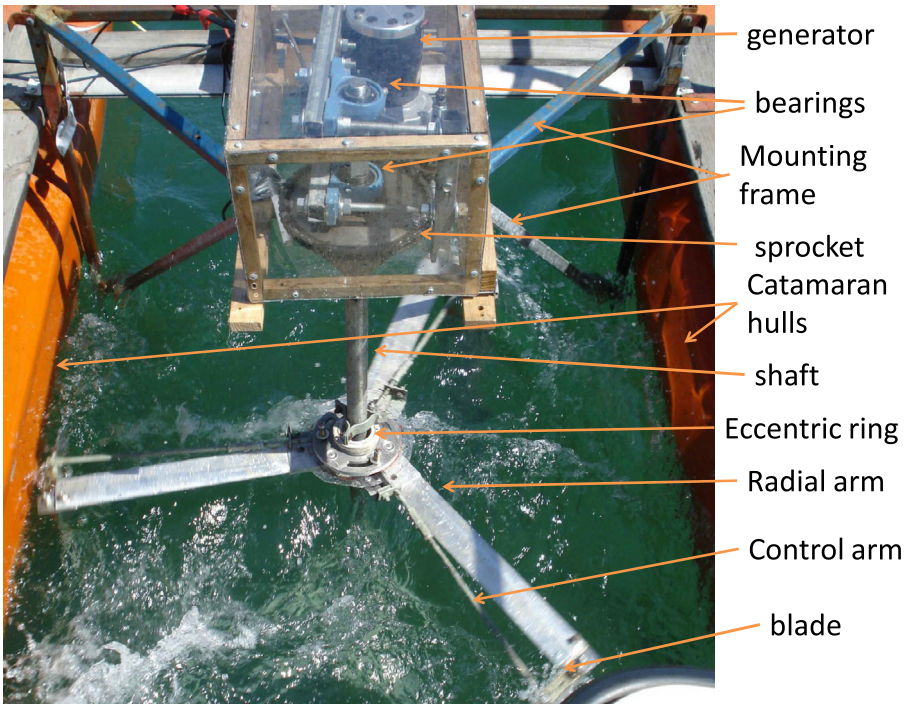

Fig. 8. The SA turbine raised so radial arms are easily visible.

clearly the limitations of the small scale, low speed testing commonly used to assess the performance of turbine designs which would be scaled up to much larger sizes and would operate in higher flow velocities with much higher Reynolds numbers in real applications. Parasitic drag is also likely to be higher in small scale models due to the higher zero lift drag coefficient of radial arms at low Reynolds numbers (see Fig. 4.)

Discussion

If a powerful enough towing vessel is available, open water tests can avoid the blockage errors and low Reynolds number issues experienced in small laboratory tanks, but there is generally some scatter in data because the water is not absolutely calm. Towing tanks are typically designed to test low drag shapes such as ship hulls, not turbines which produce high drag, so carriages are not usually designed with enough towing force capacity for adequate turbine testing, and very large towing tanks capable of testing realistic sized turbines are generally very expensive to hire.

SA open water tests

Referring to Fig. 9, the measured performance is fairly close to the predicted performance (which ignored radial arm drag loss) at λ ~ 2, but falls increasingly short as λ increases, suggesting that either (i) arm drag loss becomes increasingly important as λ increases, or (ii) the turbine was not performing quite as designed. Fig. 11 shows a sample of torque ripple measured on the 1 m turbine during one complete revolution. Three regular peaks and troughs would be expected if the pitch mechanism were working perfectly, and the fact that the peaks and troughs are irregular indicates that the pitch mechanism was not working perfectly, which could account for some of the discrepancy between predicted and measured performance.

Perhaps more important is the fact that the modeling did not include allowance for parasitic drag losses and these are discussed further in Section 8.1.1 below.

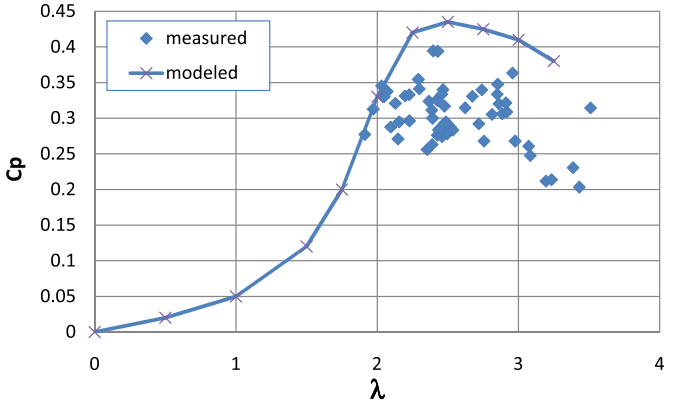

Fig. 9. SA test results. Modeled performance did not allow for radial arm drag loss.

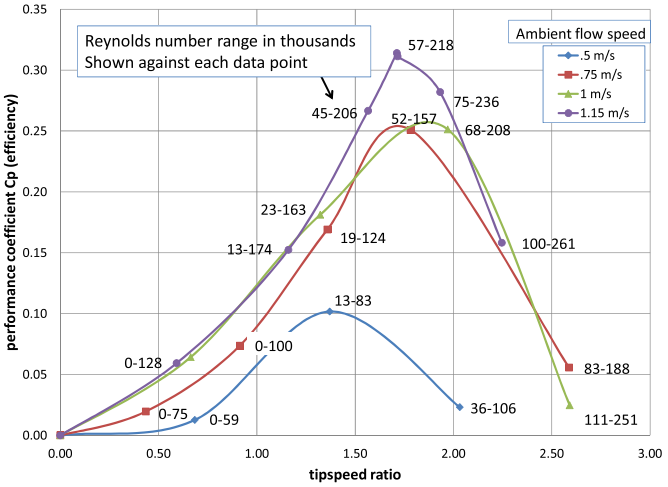

Fig. 10. UK test results: C_P–λ, V_{inf} and Reynolds number range.

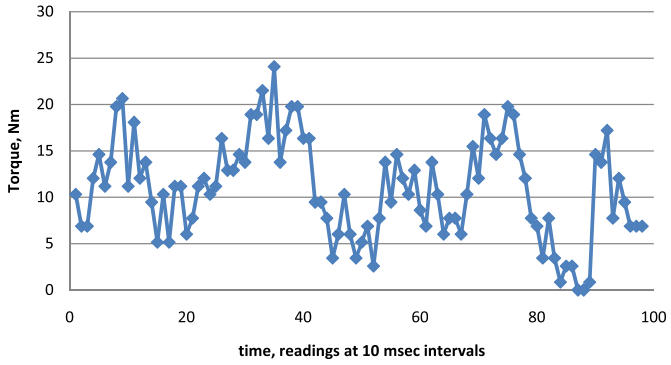

Fig. 11. Irregular torque ripple on 1 m turbine indicates that the pitch mechanism was not working perfectly.

UK towing tank tests

Channel blockage probably inflated the measured performance slightly, while friction in the cam follower may have reduced performance. Rolling contact bearings could have been used in the blade pivots and the cam follower in the UK tests, since they were short duration tests in clean water, but even expensive corrosion-resistant stainless steel bearings are prone to premature failure due to sediment in turbid water under real ocean conditions, and the aim was to design as much as possible for real conditions. Accordingly it was decided to use Vesconite, which had been readily available in Australia but proved difficult to source in the UK, and with hindsight it would have been better to use bronze bushes or sealed ball bearings for laboratory tests and deal with the issue of operating life later at the full scale prototype stage.

No modeling was done for the UK turbine but with similar geometry it would be expected to have a similar performance curve except that (i) it should peak at a slightly lower λ, which is the case, as seen in Fig. 10, and (ii) performance is very sensitive to Re at the low end of the range encountered in this work. At the lowest towing speed, 0.5 m/s, corresponding to the lowest Reynolds number range, performance is very poor. This is to be expected because symmetrical profiles like the NACA 0020 develop laminar separation bubbles at low Re below about 70,000, leading to premature stall and loss of lift. This is apparent in Fig. 4, which shows that stall angle and maximum lift coefficient decrease steeply and zero incidence drag coefficient increases steeply at low Re. All of these factors adversely affect performance.

Parasitic drag losses

Besides the adverse effects on performance of low Re, parasitic drag can drastically affect the performance of straight blade cross flow turbines, especially those with variable pitch mechanisms which consume power. The original Darrieus wind turbine was of the troposkein or "eggbeater" pattern in which blades are attached to the central shaft at top and bottom and may have no radial arms to create parasitic drag, or may have short, thin tension-only arms near the top and bottom, as shown in Fig. 12, where their speed, radius and hence drag contribution is low.

However straight blade turbines require arms to the full turbine radius to support the blades, as shown in Figs. 1 and 8. For a surface-mounted turbine it is possible to cantilever blades from arms above the surface, as done by Kaare and Evensen (2003), in which case the only parasitic drag is from air, which accounts for the very high C_P of 0.5 achieved by Kaare and Evensen (2003). However this arrangement leads to very high bending moments in blades and arms and is probably not practicable in most situations, so parasitic drag must be taken into account.

Fig. 12. Original troposkein curved blade Darrieus wind turbine: very little parasitic drag.

Drag force on a given profile increases approximately with the square of the velocity and therefore radius (not exactly, because the drag coefficient decreases with increasing velocity and Re, as shown in Fig. 4). Also the drag torque contribution of a given drag force increases with the radius, so parasitic drag due to radial arms is a much more serious problem with straight blade turbines than with troposkein turbines.

Estimate of radial arm drag losses on a straight blade turbine

Parasitic drag can be calculated as follows: The drag force dF_D on an element of radial arm of planform area dA is given by

$$dF_D = {}^1/_2 C_{D0}\ \rho\ dA\ V_{rel}{}^2 \tag{5}$$

$$V_{rel} = \omega r + V_{inf}\cos\ \theta. \tag{6}$$

Combining (5) and (6) gives

$$dF_D = {}^1/_2 C_{D0}\ \rho\ dA\ (\omega r + V_{inf}\cos\ \theta)^2. \tag{7}$$

Thus taking the density of water $\rho = 1000$ kg/m^3, the drag torque dT_D contributed by an element of the radial arm of radial length dr and chord length c is given by

$$dT_D = dF_D r = 500\ C_{D0} c\ r(\omega r + V_{inf}\cos\ \theta)^2\ dr. \tag{8}$$

The power loss dP_D due to parasitic drag on that element is given by

$$dP_D = dT_D\ \omega = 500\ C_{D0}\ c\ r\ \omega\ (\omega r + V_{inf}\cos\ \theta)^2 dr. \tag{9}$$

The average power loss P_D for the 6 complete radial arms of length R over a complete revolution is obtained by integrating (9):

$$\begin{aligned} P_D &= \frac{3000 C_{D0} c\omega}{2\pi}\int_0^{2\pi} d\theta \int_0^R r(\omega r + V_{inf}\cos\theta)^2 dr \\ &= 750 C_{D0} c\omega\left(\omega^2 R^4 + V_{inf}{}^2 R^2\right). \end{aligned} \tag{10}$$

For the UK turbine, c = 0.03 m, R = 0.25 m, $V_{inf} = 1.15$ m/s maximum, and at maximum C_p, $\lambda = 1.7$. Substituting these values

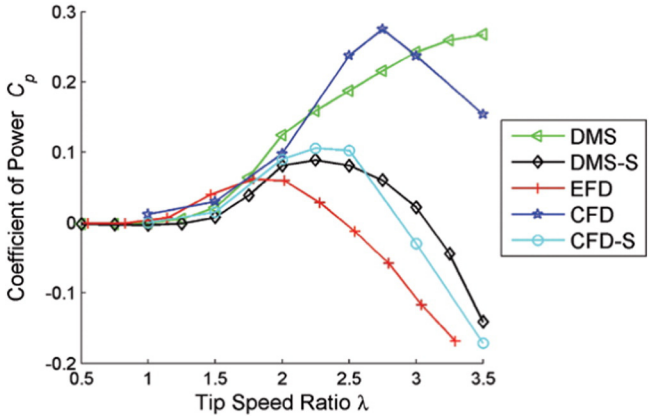

Fig. 13. CFD prediction of parasitic drag loss due to radial arms ("struts") after Rawlings (2008).

into (10) and taking $C_{D0} = 0.022$ as shown in Fig. 4 for Re = 81,000 (an approximate average figure for radial arms), give

$P_D = 750 \times 0.022 \times 0.03 \times 7.82(7.82^2 \times 0.25^4 + 1.15^2 \times 0.25^2) =$ 1.24 W total for 6 arms, only about 2% of the measured peak power output of 60 W.

For the SA turbine c = 0.06 m, R = 0.5 m, V_{inf} = 1 m/s maximum, and at maximum C_p, λ ~ 2.5. Substituting these values into (6) and taking $C_{D0} = 0.016$ as shown in Fig. 4 for Re = 163,000, give

$P_D = 750 \times 0.016 \times 0.06 \times 5(5^2 \times 0.5^4 + 1^2 \times 0.5^2) = 6.5$ W total for 6 arms.

Taking an average figure of $C_{p\ max} = 0.32$, the peak power was approximately

$P = C_p \frac{1}{2} \rho A V_{inf}^3 = 0.32 \times 500 \times 1.2 \times 1^3 = 192$ W, so parasitic loss is about 3.3% of the measured peak power output—still fairly small but higher than for the UK turbine because the SA turbine was operating at higher λ and from E. (10), parasitic drag increases approximately with Ω^3 since the value of Ω^2R^4 is much greater than V^2R^2.

Combined arm and blade-arm junction losses

Besides the losses from radial arms, there are further losses due to the blade–arm junction, and these have been predicted by Marsh et al. (2012) as shown in Fig. 13, which compares (i) CFD predictions with and without strut (arm) loss, (ii) DMS (double multiple streamtube) predictions and (iii) measured performance of a fixed pitch turbine with a radius and height of 0.482 m, 3 blades of NACA634221 section and 6 radial arms of NACA0021 section, with blade and arm chord both 0.07 m, giving $\sigma = nc/r = 3 \times 0.07/0.482 = 0.435$. Although there are some differences in geometry between this turbine and those described in the present work, they are similar enough to expect similar parasitic drag loss. Fig. 13 shows reasonable agreement between predictions and experiment up to λ ~ 2, but a rapid increase in parasitic loss as λ increases above about 2.

Fig. 14 after Rawlings (2008) shows a comparison of performance coefficient Ck (= C_P) against tsr (λ) for a turbine with 4 different radial arm arrangements under otherwise identical conditions. The turbine was 36 in. (914 mm) in diameter with 3 blades of NACA 63_4-021 section, 27 in. (686 mm) long with chord length 2.57 in. (65 mm), giving a solidity nc/r = 0.43, lower than either the Australian or the UK turbine described in this study. Curve A was measured with two 31% thick aerofoil arms attached to the blades at the quarter span points, curve B with two 21% thick approximate aerofoil arms at quarter span points. Curve C (red triangles) used three thin (NACA0012) aerofoil arms at blade ends and midspan. Curve C (green x's) used two thin (NACA0012) aerofoil arms at blade ends only. It will be apparent that both the arm section and location make a very large difference. For efficiency it is clearly preferable to place arms at the ends of the blades only, but from a structural point of view this leads to much higher bending moments, stresses and deflections.

Conclusions

The performance of two variable pitch straight blade vertical axis hydrokinetic turbines has been modeled and measured experimentally, one in open water and one in a laboratory towing tank. Two-dimensional modeling, ignoring parasitic drag losses, over-predicts peak performance coefficients C_P for turbines with simple sinusoidal pitch at around 45% and up to 49% for an optimized cam-driven pitch regime. Depending on the arrangement of the arms supporting the blades, parasitic drag losses due to arms and blade-arm junctions can be very large, and experimental C_P of small models rarely exceeds about 32%. Reynolds number effects are important for small model turbines at low flow velocities, and higher C_P may be achieved on larger turbines.

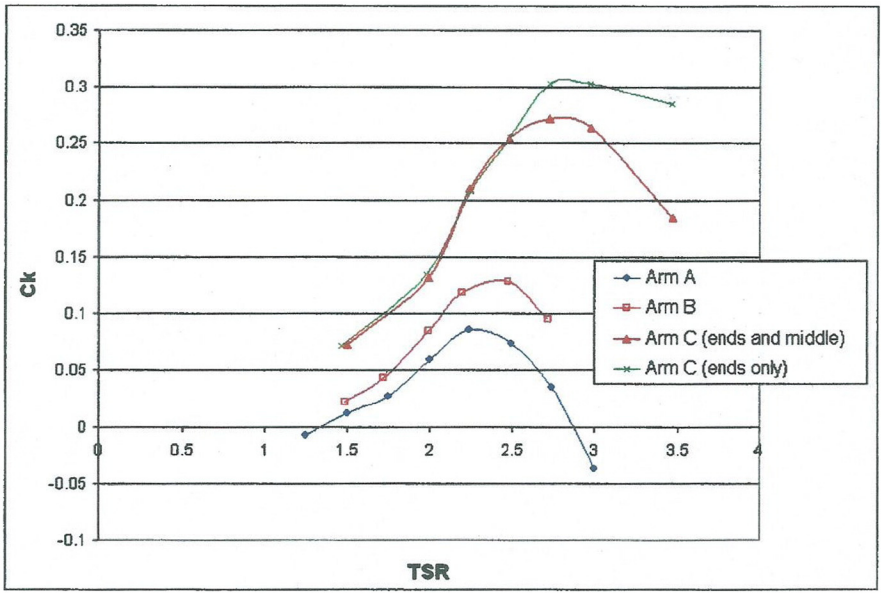

Fig. 14. Comparison of Ck (= C_P) vs tsr (= λ) for a turbine with 4 different radial arm arrangements.

Acknowledgements

The author would like to thank the following people, all of whom have contributed to the insights gained in this paper: Neil Anderson, Leo Lazauskas, Ric Capaldo, Dean Thomas, Wayne Ryan, Adrien Vigoulette, Martin Anyi, Rob Kirke, Barry Bristow, Florent Trarieux and his students at Cranfield University. Also the following organizations for financial and/or in kind support: Coastal Hydropower Corporation, BC, Canada, who financed construction of early prototypes of the SA turbine, UniSA, who funded travel to the UK, and Blue Tidal Energy, UK, who financed design and construction of the UK model.

References

Batten WMJ, Bahaj AS, Molland AF, Chaplin JR. The prediction of the hydrodynamic performance of marine current turbines. Renew Energy 2008;33:1085–96.

Brulle RV. Giromill wind tunnel tests and analysis. Proc 3rd Biennial Conf/Workshop on Wind Energy Conversion Systems, Washington, DC, Sept 19–21; 1977. p. 775–83.

Coiro DP, De Marco A, Nicolosi F, Melone S, Montella F. "Dynamic behaviour of the patented kobold tidal current turbine: numerical and experimental aspects." Czech Technical University in Prague. Acta Polytechnica 2005;45. [No. 3/2005].

Cooke SC, Willden RHJ, Byrne BW. The potential of sub-arrays to increase tidal farm power. *3rd Oxford Tidal Energy Workshop*, 7–8 April. Oxford: UK; 2014.

Jacobs EN, Sherman A. *Airfoil section characteristics as affected by variations of the Reynolds number*. NACA 23rd Annual Report, No. 586; 1937. p. 227–64.

Kaare F, Evensen E. Water Power Industries, Norway, US Patent No. 20030231951A1; 2003.

Kentfield JAC. A cycloturbine with automatic, self-regulating, blade pitch control. *Proc.4th ASME Wind Energy Symposium*; 1985. p. 147–54. [Feb.17–21].

Kirke, B.K. US Patent No. 2013045080—Cross flow wind or hydrokinetic turbines, WO2011130797.

Kirke BK, Lazauskas L. Limitations of fixed pitch Darrieus hydrokinetic turbines and the challenge of variable pitch. Renew Energy 2011;36:893–7.

Lazauskas L, Kirke BK. Modeling passive variable pitch cross flow hydrokinetic turbines to maximize performance and smooth operation. Renew Energy 2012;*45*:41–50. [*Sept*].

Lazauskas L. Unpublished modeling report for coastal hydropower corporation. BC, Canada: Nanaimo; 2008.

Marsh P, Ranmuthugala D, Penesis I, Thomas G. "Three dimensional numerical simulations of a straight-bladed vertical axis tidal turbine.". *18th Australasian Fluid Mechanics Conference*; 2012. [Launceston, Australia, 3–7 December].

Rawlings GW. Parametric characterization of an experimental vertical axis hydro turbine. BASc: University of British Columbia; 2008.

Robinson ML. The Darrieus wind turbine for electrical power generation. *J Royal Aeronautical Soc* 1981:1–9. [June].

Willden RHJ, Nishino T. Tidal stream energy: designing for blockage. *3rd Oxford Tidal Energy Workshop*; 2014. [7–8 April, Oxford, UK].